

JLAB-THY-98-47
MIT/CTP Preprint # 2799

Spin-Orbit Final-State Interaction in the Framework of Glauber Theory for $(e, e'p)$ Reactions

S. Jeschonnek¹ and T. W. Donnelly²

(1) Jefferson Lab, 12000 Jefferson Ave, Newport News, VA 23606 (2) Center for Theoretical Physics, Laboratory for Nuclear Science and Dept. of Physics, Massachusetts Institute of Technology, Cambridge, MA 02139

(October 6, 2018)

Abstract

We investigate the reactions $D(e, e'p)n$ and $D(\vec{e}, e'p)n$ at GeV energies and discuss the opportunities to distinguish between different models for the nuclear ground state by measuring the response functions. In calculating the final-state interaction (FSI) we employ Glauber theory, and we also include relativistic effects in the electromagnetic current. We include not only the central FSI, but also the spin-orbit FSI which is usually neglected in $(e, e'p)$ calculations within the Glauber framework and we show that this contribution plays a crucial role for the fifth response function. All of the methods developed here can be applied to any target nucleus.

25.30.Fj, 24.10 -i, 25.10+s

I. INTRODUCTION

Currently, there are many exclusive electron scattering experiments being performed or in the planning stage at medium to high energies, e.g. at TJNAF (Jefferson Lab), Bates, NIKHEF and MAMI. A sketch of the typical reaction is provided in Fig. 1. In treating the problem theoretically, ideally one would use a microscopic Hamiltonian for the description of both the nuclear bound state and the — in general rather complicated — hadronic final state. Such a microscopic Hamiltonian would also contain a minimal coupling to the photon, so that the initial state, final state and electromagnetic current operator would all be treated consistently in a microscopic, relativistic fashion. In practice, it is very difficult to perform a consistent calculation of both nuclear ground state and final hadronic scattering state and, especially for medium and heavy nuclei, it is unlikely that a consistent, fully microscopic and therefore relativistic treatment will be available in the near future.

At present, there are several approximate calculations for particular electronuclear reactions available for few-body systems [1–3]. However, it is difficult to extend these approaches for the few-body systems to energies above the pion emission threshold. Given the considerable effort that one expects will be put into experimental studies in this field, in the next few years calculations in the few GeV regime for reactions at least with deuteron targets will hopefully become available, although even this is not trivial. For heavy nuclei, there are only relativistic mean-field calculations available.

Therefore, at present in practice one is forced to split the problem up into three separate parts, namely the calculation of the ground state, the calculation of the final hadronic state and the treatment of the electromagnetic current. Although the approaches taken for those different parts will not be consistent, there is a good chance that by doing the best possible job for each separate ingredient, one will be able to incorporate the essential physical features in the theoretical description of exclusive electron scattering at high energies. For the nuclear ground-state wave function one either uses a solution of a bound-state Schrödinger equation or one of the more sophisticated microscopic few-body wave functions which are now available [2,3]. The final state is typically calculated using optical potentials or multiple scattering theory. It is our aim to focus on two parts of the problem: the electromagnetic current and the final state. The relativistic effects in the electromagnetic current operator have been investigated elsewhere [4] and were found to be quite important. They are included in all of the calculations presented in this paper. We will discuss methods that are applicable to all nuclei in a wide range of energies. We develop and test these methods for the case of electron scattering on the deuteron so that these effective methods can be checked against the results of microscopic calculations, once the latter are available.

This paper is organized as follows: after this brief introduction in Sec. I, in Sec. II we summarize different theoretical models for the deuteron wave function and indicate what is expected for the Plane Wave Impulse Approximation (PWIA). In Sec. III, we consider the effects of final-state interactions (FSI) and their description at high energies by Glauber theory. We discuss the different effects of central and spin-orbit FSI, which are due to their different spin-structure and to their different ranges. Then in Sec. IV we discuss the various possible choices of parameters for the FSI calculation and end in Sec. V with a brief summary and outlook.

II. MODELS FOR THE NUCLEAR GROUND STATE AND THE PWIA

Before we discuss the incorporation of FSI and the suitability of specific observables for the discrimination between different theoretical models, we would like to recall the differences between these models. There exist several models of the nucleon-nucleon interaction which are based on meson-exchange potentials [5–7] that not only make predictions for the deuteron wave function, but also describe a wide range of free NN and meson-nucleon scattering data. Recently, more microscopic approaches have been developed [2,3]. The main difference between the meson-exchange models lies in the different D-wave probability incurred: for instance, the Bonn model predicts a lower D-state probability than most other models. There are also some differences in the very short range part ($r < 0.5$ fm) of the S-wave. For the later discussions, we compare results for the Bonn wave function [5] and the Paris wave function [6], as they are good representatives for the available models and as most other theories will fall in between them.

In PWIA, the $(e, e'N)$ cross section is proportional to the product of the electron-nucleon half-off-shell cross section times the spectral function $S(E, \vec{p})$, which gives the joint probability to find a nucleon of energy E and momentum \vec{p} in the nucleus:

$$\frac{d^6\sigma^{PWIA}}{d\epsilon' d\Omega_e d\Omega_N dE_N} = K\sigma_{eN}S(E, \vec{p}), \quad (1)$$

where K is a kinematic factor and σ_{eN} is the electron-nucleon half-off-shell cross section. In the case of the deuteron, the energy E is fixed by the binding energy and the spectral function reduces to the momentum distribution $n(p)$ which does not depend on the direction of the momentum \vec{p} , as long as unpolarized deuterium is considered. Different predictions for the momentum distribution $n(p)$ are shown in Fig. 2a. It should be noted that although the discrepancy for higher momenta is large — up to a factor of five — the momentum distribution varies over seven orders of magnitude, and the agreement between the models is quite good overall. It is interesting and important to glean information on the high momentum part of $n(p)$ from experiment, as it is this kinematic region that is expected to tell us about the transition from hadronic degrees of freedom to quark-gluon degrees of freedom.

The different predictions for momenta $p > 1.5$ fm $^{-1}$ stem from the different D-wave probabilities: in Fig. 2b, the decomposition of the momentum distribution into S-wave and D-wave is shown, and one can see clearly that the momentum distribution is dominated by the D-wave for momenta of 1.5 fm $^{-1}$ and higher.

Of course, the simple picture of PWIA is only an approximation, as the outgoing nucleon will in fact interact with the residual system, and this interaction will break the simple factorized relation of Eq. (1) involving the single-nucleon cross section and nuclear spectral function. This means that the momentum distribution cannot be extracted from the data immediately; in fact, it is a difficult problem to find observables which show sufficient sensitivity to the different models of the ground-state wave function. In the following, we will discuss some possible candidates.

III. FINAL-STATE INTERACTION

Here we are interested in scattering in the GeV energy regime, and the natural description of the FSI in this regime is given by Glauber theory [8]. Let us briefly recall the change of the nature of the NN interaction that occurs in going from low to high energies. At energies of 100 MeV or less, the scattering of nucleons is elastic and nearly isotropic and only a few partial waves contribute, while in contrast, at high energies, the interaction becomes absorptive, as new particles are produced. At an energy of 500 MeV, the proton-proton inelastic cross section rises sharply from values of less than 2 mb to approximately 30 mb (for a review, see [9]). It then remains almost constant for energies up to several hundred GeV. The NN interaction also becomes diffractive at high energies. The proton-nucleus elastic scattering data (see e.g. [10,11]) taken at proton beam energies of 1 GeV and higher show a clear diffractive pattern, with broad maxima and diffractive dips, reminiscent of the patterns obtained in optics in Fraunhofer diffraction. In the past, there have been great successes in the description of proton-nucleus scattering data with Glauber theory, see e.g. [10–12], and we will apply it here — with the necessary modifications — to the $(e, e'N)$ reaction.

Once FSI is included, the generic form of the matrix elements we have to calculate is $\mathcal{M}_{fi} = \langle f | S J_{em} | i \rangle$, where J_{em} denotes the current operator and S is the FSI operator discussed below. An overview of the conventions used in this paper and the relativistic current operator employed in our calculations can be found in the appendix. The FSI operator $S(\vec{r})$ for the interaction between the outgoing nucleon and a spectator nucleon reads

$$S(\vec{r}) = 1 - \theta(z) \cdot \Gamma(\vec{b}), \quad (2)$$

where the distance \vec{r} between the two interacting nucleons is decomposed into longitudinal and transverse parts: $\vec{r} = \vec{b} + z \cdot \hat{q}$, where \hat{q} indicates the direction of the virtual photon's momentum. The θ -function indicates that the spectator nucleon has to be in the forward hemisphere with regard to the struck nucleon, otherwise no FSI will take place. $\Gamma(\vec{b})$ is called the profile function of NN scattering, and is related to the NN scattering amplitude $f(\vec{l})$ via the Fourier transform:

$$\Gamma(\vec{b}) = \frac{1}{2\pi ik} \int d^2 \vec{l} \exp(-i\vec{l} \cdot \vec{b}) f(\vec{l}). \quad (3)$$

Here \vec{k} is the incident nucleon momentum, \vec{k}' denotes the outgoing nucleon's momentum, and $\vec{l} = \vec{k} - \vec{k}'$ is the momentum transferred in the NN scattering (not to be confused with the momentum \vec{q} transferred to the nucleus by the electron). The most general form for the scattering amplitude in the NN center of mass (c.m.) system assuming parity conservation, time-reversal invariance, the Pauli principle, and isospin invariance can be written in terms of five invariant amplitudes (see references given in [9]):

$$\begin{aligned} f(\vec{l}) = & A(\vec{l}) + B(\vec{l}) (\vec{\sigma}_1 + \vec{\sigma}_2) \cdot \hat{n} + C(\vec{l}) (\vec{\sigma}_1 \cdot \hat{n}) (\vec{\sigma}_2 \cdot \hat{n}) + \\ & D(\vec{l}) (\vec{\sigma}_1 \cdot \hat{m}) (\vec{\sigma}_2 \cdot \hat{m}) + E(\vec{l}) (\vec{\sigma}_1 \cdot \hat{h}) (\vec{\sigma}_2 \cdot \hat{h}). \end{aligned} \quad (4)$$

The nucleon spin operators are denoted by $\vec{\sigma}_1$ and $\vec{\sigma}_2$, and $\hat{n} \equiv \vec{k} \times \vec{k}' / |\vec{k} \times \vec{k}'|$, $\hat{m} \equiv (\vec{k} - \vec{k}') / |\vec{k} - \vec{k}'|$, and $\hat{h} \equiv (\vec{k} + \vec{k}') / |\vec{k} + \vec{k}'|$.

In principle, the amplitudes A , B , C , D and E can be determined from a complete phase shift analysis of NN data. In practice, for Glauber theory calculations one chooses a parameterization of the central amplitude, A , in terms of three experimentally known parameters: the total NN cross section, the diffraction slope b_o^2 and the ratio ρ of the real to imaginary parts of the elastic forward scattering amplitude. We discuss the differences between these approaches later in Sec. IV. For the following discussion, we employ the latter approach, writing

$$A(l) = \frac{k \sigma_{tot}^{NN}}{4\pi} (\rho + i) \exp(-0.5 l^2 b_o^2). \quad (5)$$

Note that sometimes this amplitude is parameterized as

$$A = A_o \cdot \exp(-\beta_A l^2), \quad (6)$$

where A_o and β_A are complex numbers, leading to a profile function of the form

$$\Gamma(\vec{b}) = \frac{\sigma_{tot}^{NN}(1 - i\rho)}{4\pi b_o^2} \exp\left(-\frac{\vec{b}^2}{2b_o^2}\right). \quad (7)$$

For a 1 GeV nucleon, $b_o \approx 0.5$ fm and accordingly the profile function changes on a scale that is much smaller than the nuclear radius, i.e., approximately 2 fm for the deuteron. This means that the central FSI operator is a short-ranged function with respect to the transverse separation of the nucleons and a long-ranged function with respect to their longitudinal separation.

In the analysis of the proton-nucleus scattering data, the spinless version of Glauber theory, including only the central part of the NN interaction, was very successful [10,11]. We also start by including only the central part, as was done before in [13,14].

A. Central FSI

Before we start the discussion of the results including FSI, some remarks about conventions and the choice of kinematics are in order. We plot our results versus the missing momentum $\vec{p}_m = \vec{q} - \vec{p}_N$, where \vec{q} is the momentum transferred to the nucleus by the electron and \vec{p}_N is the momentum of the detected nucleon in the final state. In PWIA, it coincides with the negative initial momentum of the struck nucleon inside the nucleus: $\vec{p}_m = -\vec{p}$. We denote the angle between \vec{p}_m and \vec{q} by θ , and the term “parallel kinematics” indicates $\theta = 0^\circ$ and “perpendicular kinematics” indicates $\theta = 90^\circ$. In this paper, we assume that the experimental conditions are such that the kinetic energy of the outgoing nucleon and the angles of the missing momentum, θ and the azimuthal angle ϕ , are fixed. The kinetic energy T_p of the outgoing proton is fixed to 1 GeV. For changing missing momentum, the transferred energy and momentum change accordingly. Fig. 3 shows the five-fold differential cross section for the reaction $D(e, e'p)n$ in parallel kinematics (left panel) and for perpendicular kinematics (right panel). In perpendicular kinematics, the effect of the central FSI is most pronounced: for missing momenta from 0.8 fm^{-1} to 1.5 fm^{-1} , the FSI reduces the cross section, and for missing momenta higher than 1.5 fm^{-1} , it drastically enhances the cross section, by up to

an order of magnitude. The central FSI effects in parallel kinematics are smaller, but still important for higher missing momenta.

Fig. 4 shows the cross section in PWIA and with central FSI, calculated using the Bonn and the Paris wave functions. Whereas the predictions of the two models differ for PWIA for higher missing momenta, the curves become almost indistinguishable in perpendicular kinematics and very similar in parallel kinematics once the FSI effects are included. These results can be understood when we consider the properties of final-state interactions: they are short-ranged, and this means that while they act on the S-wave, their effect on the D-wave is small, as the D-wave is suppressed at short distances by the centrifugal barrier. In the discussion of Fig. 2, we have seen that the difference between the models at higher momenta stems from their different D-wave content, and that the D-wave dominated the momentum distribution at higher momenta. Once FSI are included in the calculation, they redistribute S-wave strength from low and medium missing momenta to high missing momenta, so that with FSI, the S-wave becomes important for this kinematic region. As the wave function models do not differ too much in the S-wave, the cross sections calculated with the two models including FSI effects do not differ very much, either. These issues have been discussed in greater detail in [13].

Thus, the unpolarized $D(e, e'p)n$ cross section is not a good candidate for the experimental discrimination between theoretical models. The central FSI effects in the longitudinal and transverse response functions are fairly similar to the FSI effects in the cross section (for the convenience of the reader, the definition of the response functions and the different components of the current operator is given in the appendix). This comes as no surprise, because R_L is dominated by the zeroth-order charge operator and R_T is dominated by the magnetization current. Their coordinate space structure is the same apart from different multiplicative factors, the main difference being in the spin-operator structure. As we are considering only central FSI at this moment, the FSI effect in the two sectors will be the same.

In order to find a better suited observable for the study of the nuclear ground state, we turn our attention to the smaller interference responses, R_{TT} and R_{TL} , which have a different structure than the larger responses R_L and R_T . Since the former vanish in (anti)parallel kinematics, in Fig. 5 we show them only in perpendicular kinematics. One should note that the transverse-longitudinal response R_{TL} is considerably smaller than R_L and R_T , and that in turn the transverse-transverse response R_{TT} is much smaller than R_{TL} . We remark that the separation of the interference responses from the measured cross section is by no means easy; here, we focus on discussions of their properties, disregarding the experimental feasibility for the moment.

In panels (a) and (c) of Fig. 5 we show R_{TT} and R_{TL} calculated in PWIA (dashed line) and including central FSI (solid line); in panels (b) and (d), we show the responses calculated with central FSI decomposed into their S-wave (dashed line) and D-wave (dash-dotted line) components.

First, we discuss R_{TL} , shown in panels (a) and (b) of Fig. 5. Starting at missing momenta of 1 fm^{-1} , the transverse-longitudinal response shows a strong FSI effect: at first, the response is reduced by final-state interactions, then, for $p_m > 2.2 \text{ fm}^{-1}$, it is enhanced. The overall behavior of the FSI effect is similar to that in the cross section and in R_L and R_T , but the enhancement due to FSI sets in at higher missing momentum — for the cross

section, it starts at $p_m > 1.5 \text{ fm}^{-1}$. The decomposition of the response into S-wave and D-wave components, as shown in panel (b), exhibits a unique feature of R_{TL} in that even with the final-state interactions included, the D-wave plays a prominent role and at medium missing momenta, $1.2 \text{ fm}^{-1} < p_m < 2.3 \text{ fm}^{-1}$, it is much larger than the S-wave contribution. This does not happen in the longitudinal response [13] or in the transverse response. The D-wave is scarcely affected by FSI, and only when the S-wave contribution becomes larger than the D-wave contribution does the typical enhancement of the response in perpendicular kinematics due to FSI set in.

The transverse-transverse response R_{TT} shows only a small effect of FSI, namely, a slight reduction at medium missing momenta. Fig. 5 (d) explains why: for missing momenta $p_m > 1.5 \text{ fm}^{-1}$, the response is entirely given by the D-wave contribution, while the S-wave is negligible for medium missing momenta and increases again only for $p_m > 3 \text{ fm}^{-1}$, a region where the whole response is small. Since the central FSI are short-ranged, they do not affect the D-wave very much — see the discussion above — and therefore the FSI effects on R_{TT} are small.

So at this stage, it seems that, if they could be determined experimentally, the interference responses might be well-suited for an experimental discrimination between different theoretical models for the nuclear ground state, as they differ mainly in their D-wave content and both R_{TT} and R_{TL} show sensitivity to it. However, here we have to be careful and review the approximations which went into our calculation so far. One has to keep in mind that the interference responses are much smaller than the longitudinal response R_L and the transverse response R_T , and that R_{TT} roughly accounts for only 1% of the total cross section, and R_{TL} is not much bigger. So any additional contribution that would be a 1% effect on the total cross section, and which might therefore be neglected with good reason in the calculation of the cross section, could give rise to a huge effect in the interference responses, especially in R_{TT} . For example, meson-exchange current effects (which are not considered in the present work) may play such a role.

One of the reasons why the transverse-transverse response is so small is that in PWIA the magnetization current cannot contribute, unless one includes a second-order relativistic correction to the current, see [4], with which it can interfere. Recalling that $R_{TT} = 2\Re[J_+^* J_-]$ and taking into account that for the magnetization current, J_\pm contains the spin-flip operator σ_\pm , it is easy to see that for the S-wave, the magnetization current cannot contribute, unless there is a spin-dependent, spin-flipping FSI. This means that, although it is quite reasonable and has been common successful practice to use only a central final-state interaction within the framework of Glauber theory in the calculation of cross sections, it is not appropriate to neglect the spin-dependent FSI in the calculation of certain responses, in particular in the calculation of the interference responses discussed here. We now proceed to address this issue.

B. Spin-dependent FSI

The NN amplitude in Eq. (4) contains one spin-orbit term and three double-spin-flip terms. The unique determination of these contributions to the NN amplitude is more difficult than for the central part, and especially the double spin-flip terms are hard to obtain. Due to their different spin structure the spin-orbit term and the double spin-flip

terms have different effects on the $(e, e'p)$ observables, so that a separate discussion of them is justified. Here, we concentrate on the spin-orbit term. It may be parameterized as

$$B(l) = \gamma \frac{k \sigma_{tot}^{NN}}{4\pi} (\rho_s + i) l \exp(-0.5 l^2 b_s^2). \quad (8)$$

The corresponding profile function reads:

$$\Gamma_s(\vec{b}) = -i \gamma \frac{\sigma_{tot}^{NN}}{4\pi b_s^4} (1 - i\rho_s) b \exp(-\frac{b^2}{2b_s^2}), \quad (9)$$

so that we have for the full profile function defined in Eq. (3)

$$\Gamma(b) = \Gamma_c(\vec{b}) + \Gamma_s(\vec{b}) \sigma \cdot \nu, \quad (10)$$

with $\nu = \hat{b} \times \hat{k}$. Comparing the expression for the spin-orbit amplitude with that for the central amplitude, the main difference is in the functional form of the former: it contains a factor l , where l is the transferred momentum, and this makes the corresponding spin-orbit profile function $\Gamma_s(\vec{b})$ a longer-ranged function than the short-ranged central profile function $\Gamma(\vec{b})$. In addition, the value of b_s is larger than that of b_o used for the central amplitude, further increasing the longer range of the spin-orbit amplitude. The value for $\gamma \approx 0.16$ fm taken from [12] indicates that the absolute value of the spin-orbit amplitude is much smaller than the central contribution. This indicates that the contribution of the spin-orbit final-state interaction will be significant only if it interferes with the central FSI.

To illustrate these points, in Fig. 6 we compare the real and imaginary parts of the central profile function (solid line) and the spin-orbit profile function (dashed line) for $p - n$ scattering. We use the parameters $\sigma_{tot}^{pn} = 41.1$ mb, $b_o = 0.48$ fm and $\rho = -0.48$, while for the spin-orbit part we use $\gamma = 0.16$ fm, $b_s = 0.65$ fm and $\rho_s = -0.24$. These parameters are the average of the parameters quoted in Table 10 of Ref. [11] for Glauber theory analyses at $T_{lab} = 1$ GeV. For the real parts of the profile functions, shown in panel (a), the central contribution is dominant for transverse separations $b < 1.6$ fm, then falls off quite fast and at $b \geq 2.5$ fm is two orders of magnitude smaller than the spin-orbit contribution. However, at these larger separations, the most important contribution stems from the imaginary part of the spin-orbit profile function; see panel (b). It dominates the central contribution already for $b > 1$ fm, and remains quite large for larger b . We note that there are even larger values for b_s published in the literature, e.g. a value of $b_s = 0.81$ fm in [12], and that, if one substitutes one of these for our smaller value of $b_s = 0.65$ fm, the spin-orbit profile function will be enhanced significantly at larger b .

In the following, we investigate the consequences of the longer-range character and different spin structure of the spin-orbit profile function. For the cross section and the two large responses, R_L and R_T , the influence of the spin-orbit FSI is — as expected — very small. The simple structure of the longitudinal response, $R_L = |\rho|^2$, and transverse response, $R_T = |J_+|^2 + |J_-|^2$, does not restrict any kind of contribution even with central FSI, and therefore, by including the spin-orbit FSI which would allow for different spin structures to contribute, no strength is gained. The results with and without spin-dependent FSI almost coincide, and therefore we do not show them here.

The situation changes once we consider the interference responses. They are shown in Fig. 7. On the left-hand side, the responses R_{TT} and R_{TL} are shown calculated with the full

FSI (solid line), with central FSI only (dashed line), and without FSI (dash-dotted line). For the transverse-longitudinal response, the additional spin-orbit FSI has only a marginal effect on the result for missing momenta from 1.8 fm^{-1} to 3.5 fm^{-1} . Therefore, also the decomposition into S-wave and D-wave contributions is practically unchanged compared to the central FSI results.

For the transverse-transverse response, the spin-orbit FSI plays an important role. The results for PWIA, i.e. no FSI at all, and for central FSI are very similar; they show a smooth, structureless decrease with increasing missing momentum, and the response is negative for the entire p_m range. Once the spin-orbit FSI is included, the response starts out negative at small missing momenta, then changes sign at $p_m = 1.2 \text{ fm}^{-1}$, and becomes negative again at $p_m = 1.5 \text{ fm}^{-1}$. For higher missing momenta $p_m > 2 \text{ fm}^{-1}$, the spin-orbit FSI increases the response significantly. This is due to the fact that with the spin-dependent FSI, the magnetization current now can also have an S-wave contribution to R_{TT} . Without spin-dependent FSI, this contribution does not exist. As the magnetization current is the largest contribution to J_+ and J_- , and as the S-wave is the largest component of the deuteron wave function, the new contribution introduced by the spin-orbit FSI is obviously important. This is demonstrated in Fig. 7 (d), where the full transverse-transverse response is decomposed into S-wave (dashed line) and D-wave (dash-dotted line) contributions. The S-wave contribution is larger than the D-wave contribution for all missing momenta, and it is dominant for $p_m > 2 \text{ fm}^{-1}$. This is in sharp contrast to the picture for central FSI only (compare with Fig. 5 (d)): there, the S-wave contribution is much smaller than the D-wave for $p_m > 2 \text{ fm}^{-1}$, while it is practically negligible in the region from 2 fm^{-1} to 2.5 fm^{-1} . Indeed, the increase in the S-wave part in this region amounts to more than 1.5 orders of magnitude. The effect of the spin-orbit FSI on the S-wave part can be attributed to the spin structure changing nature of the FSI.

There is another interesting spin-orbit FSI effect here which originates in its longer range, namely, the effect on the D-wave. As mentioned above and discussed in detail in [13], the central FSI does not affect the D-wave very much, as it is short-ranged and the D-wave is suppressed at short distances by the centrifugal barrier. However, the spin-orbit FSI has a longer range, and if we compare the D-wave part of R_{TT} with central FSI (Fig. 5 (d)) and with central + spin-orbit FSI (Fig. 7 (d)), there is a dramatic difference: the latter causes the D-wave part to be positive over the entire p_m range, whereas with central FSI only, the D-wave part is positive for missing momenta less than 0.5 fm^{-1} and turns negative afterwards. The absolute magnitude is affected as well by the spin-orbit FSI: it introduces a dip around $p_m = 2.2 \text{ fm}^{-1}$, whereas with the central FSI it just decreases smoothly. This is the first instance we encounter where the FSI changes the D-wave contribution significantly. In combination with the effect of the spin-orbit FSI on the S-wave, this leads to an inversion of the importance of the two contributions for R_{TT} . This is very important, as the ability to discriminate experimentally between different theoretical models for the nuclear ground state depends on being sensitive to the D-wave, in which the model predictions differ.

This leads to the last point in our discussion of the interference responses: the comparison of the different model wave functions. In Fig. 8, in panels (a) and (c), we show the transverse-longitudinal and transverse-transverse responses in PWIA, calculated with the Bonn wave function (solid line) and the Paris wave function (dashed line). As expected, the results differ at higher missing momentum where we have seen that the D-wave plays an important

role. Once the full FSI, including central and spin-orbit interactions, is included in the calculation, R_{TL} is affected at higher missing momenta; however, it basically retains its potential for discrimination between the different ground-state wave functions. This is due to the fact that for R_{TL} , the D-wave is an important contribution for $p_m > 1.3 \text{ fm}^{-1}$. For the transverse-transverse response, the difference in the PWIA results is roughly the same as for R_{TL} . However, the full FSI alters the picture: for higher missing momenta, $p_m > 2 \text{ fm}^{-1}$, the Bonn and Paris wave functions give very similar results. At medium missing momenta, $1 \text{ fm}^{-1} < p_m < 1.8 \text{ fm}^{-1}$, the sensitivity to the models is increased by FSI. This is the region where S-wave and D-wave contributions have similar size. Unfortunately, the practical use of this information is limited: from the experimental point of view, a separation of R_{TT} is very difficult, as this is the smallest of the four responses generally present in the unpolarized $D(e, e'p)n$ reaction, and the experimental errors might be largest in the region of $1 \text{ fm}^{-1} < p_m < 1.8 \text{ fm}^{-1}$, which includes two zeros of the response. From the theoretical point of view, it is advisable to include the full relativistic electromagnetic current for the calculation of R_{TT} , see [4], and it is possible that meson-exchange currents may play a role, too. In this paper, it is our goal to demonstrate that even in the GeV energy regime, it is mandatory to include spin-dependent FSI effects, although we do not claim to have treated the reaction mechanism fully.

We now turn to the fifth response function, $R_{TL'}$, which can only be measured with a polarized electron beam and vanishes for PWIA. Its dependence on the out-of-plane angle φ is given by $\sin \varphi$, and therefore we consider this response at an out-of-plane angle $\varphi = 90^\circ$. Fig. 9 (a) shows $R_{TL'}$ calculated with the full FSI (solid line) and with the central FSI (dashed line). With central FSI, the response is positive up to $p_m = 2.6 \text{ fm}^{-1}$ and then changes sign. Once the spin-orbit FSI is included, the response is negative for $p_m < 1.4 \text{ fm}^{-1}$ and becomes positive afterwards. Also, the magnitude is changed drastically by the spin-dependent FSI: for small missing momenta, $R_{TL'}$ is increased by a factor of four and more. For the higher missing momenta, the response is increased by more than one order of magnitude. Being rather large, this is likely to be an observable effect, and it shows clearly that for polarization observables such as the fifth response function the inclusion of spin-dependent FSI is absolutely necessary.

In Figs. 9 (b) and (d), we show the decomposition of the full wave function into S- and D-wave contributions, for the full FSI in panel (b) and for central FSI only in panel (d). In both cases, the S-wave is the most prominent contribution, especially for the full FSI calculation, where the influence of the D-wave is reduced to the region around $p_m \approx 1.3 \text{ fm}^{-1}$, i.e., where the S-wave contribution changes sign. In the central FSI calculation, the D-wave contribution is slightly more important, as its size is larger than for the full FSI result and as the absolute magnitude of the S-wave contribution is smaller than for the full FSI at higher missing momenta. Consequently, the difference between the Bonn and Paris wave function results is marginal; see Fig. 9 (c), where the full line represents the Bonn result and the dashed line represents the Paris result. The two curves are almost on top of each other.

The large differences between the full FSI and central FSI results stem from the different spin-structure of the spin-orbit FSI operator. For central FSI, there are two contributions in the S-wave: the largest is given by the magnetization current and the spin-orbit charge operator, and the convection current and the zeroth-order charge operator yield a contribu-

tion of different sign and approximately half the magnitude of the magnetization/spin-orbit contribution (for an extensive discussion of the electromagnetic current see [4]). Once the spin-orbit FSI is included, the previously existing contributions are unchanged, but there arise new contributions, the dominant new contribution being the one coming from the magnetization current and the zeroth-order charge operator. It is about 40% larger than the magnetization current/spin-orbit charge operator result, and it has a different sign. This new contribution is responsible for changing the sign and increasing the magnitude of the S-wave contribution to the fifth response. There are also new contributions involving the interference of the convection current with the spin-orbit charge operator and the first-order convective spin-orbit current which did not contribute at all for the central FSI, although these contributions are small. The main effect is that the two biggest components of the current, the zeroth-order charge operator and the magnetization current, can interfere with each other and contribute due to the spin-orbit FSI, and therefore change the character of the fifth response.

Previous calculations employing Glauber theory for $(e, e'p)$ reactions at high energies only took into account central FSI [13–16], which is reasonable when one is interested in the cross sections, large responses and nuclear transparencies. However, the measurement of the smaller responses and of the polarization observables is expected to reveal most about the nuclear wave function, and so the inclusion of spin-orbit FSI will be necessary for the interpretation of the experimental data. There is also a recent publication [17] in which both central and spin-orbit FSI are treated within a Dirac eikonal formalism. Although spin-orbit FSI in [17] is also found to be important for certain polarization observables and in R_{TT} , its effects in the fifth response are small. This may be due to the consideration of a different target nucleus, ^{16}O , or due to the different approach used there.

IV. INFLUENCE OF THE NN PARAMETRIZATIONS

In this section, we discuss the different parametrizations for the NN amplitude and the effects of changes in these parameters on the results we have obtained. For the central part of the amplitude, this has been done before in [18]. There, it was shown that changes in the slope parameter b_o affect the results in perpendicular kinematics, increasing them for high missing momenta if b_o is smaller and the interaction therefore shorter-ranged, and decreasing them at high p_m if b_o is chosen larger. In any case, the results with FSI lead to a considerably larger high missing momentum tail than in PWIA. A change in ρ , the ratio of the real to imaginary parts of the forward elastic scattering amplitude, influences the results only in parallel and antiparallel kinematics.

The spin-dependent part of the amplitude is not known as well as the central part, and there are many different values for the spin-orbit parametrization to be found in the literature (for an overview, see [11]). The two main groups are the values derived from phase shift analyses and from proton-nucleus Glauber theory calculations. In the Glauber approach, one usually neglects all double-spin-flip contributions and in addition assumes that the slope parameters are real, in contrast to the complex values derived in the phase shift analyses. Actually, the two different approaches already differ quite significantly in the central part: the diffraction slope derived in a typical phase shift analysis is about 50% larger than the one derived from Glauber calculations. Characteristic values at $T_{lab} = 1$ GeV are listed in

Tables I and II. The phase shift values are taken from [19], while the Glauber values are the average of the parameters quoted in Table 10 of Ref. [11]. Except for ρ_s , which enters in the spin-orbit part, all of the parameters agree within 10 – 20%. As already mentioned, the parameters b_o and b_s of the phase shift analysis have an imaginary part, although it is small. For ρ_s , there is a wide spread of values even among the different Glauber analyses, yielding values from 0.4 to –0.62. Clearly, we need to investigate how much a change in this parameter affects our results.

The situation is somewhat more complicated by the fact that the final-state interaction is not calculated in the NN c.m. system, for which the parametrizations are given, but in a system where the incoming and outgoing nucleons all have different momenta: before the FSI takes place, the proton carries the sum of its initial momentum and the momentum \vec{q} transferred by the photon, and the neutron still carries the momentum it had initially in the deuteron. After the FSI took place, the neutron carries the missing momentum \vec{p}_m , and the proton has the momentum \vec{p}_N . As the proton’s momentum is high in any case, and the neutron’s initial momentum on the average will be smaller than the Fermi momentum ($p_F \approx 55$ MeV for the deuteron), the situation is rather asymmetric. At least for the deuteron, the rescattering takes place in a system quite close to the lab system, as the Fermi momentum is so small.

Therefore, we have to boost the NN parameters from the c.m. system to the appropriate “rescattering system”. As in the rescattering system the momenta of the nucleons do not transform into one another under time reversal, we pick up different coefficients C_1 and C_2 for the spin-orbit part for the two different nucleons. This is in analogy to the transformation from the c.m. frame to the Breit frame, which was discussed in [11,19]. We have transformed the NN parameters to the lab frame, since taking into account the nonvanishing initial momentum of the neutron would only lead to negligible additional corrections. We used the method outlined in [19] for the boost. It is well known that the central parameters do not change in a transformation from the c.m. to the lab system, provided they are multiplied with the properly boosted quantities in each reference frame [20]. This leaves the spin-orbit parameters (and also the double-spin-flip terms, which we do not consider here). The spin-orbit parameters now differ for the two nucleons, and the slope parameters pick up an imaginary part. However, we carried out a calculation with the imaginary parts of b_s set to zero and found that the results practically coincide with the results obtained for the nonvanishing imaginary parts. The spin-orbit values for the lab system obtained from the Glauber $p - A$ analysis are shown in Table III. It is obvious that the boost to the lab system has a very small effect on γ and b_s . The boost has a significant effect only on ρ_s , which is almost zero for the neutron and takes on about twice its c.m. frame value for the proton. The spin-orbit values for the lab system obtained from the phase shift analysis are shown in Table IV. Again, the boost effects are significant only for ρ_s .

Instead of discussing the merits of the Glauber $p - A$ analysis versus the phase shift analysis parameters, we investigate the sensitivity of the final results to changes in the NN parameters. From the preceding paragraph, it is clear that we have to consider moderate changes in γ and b_s , and large changes in the less well known ρ_s . As γ simply multiplies the spin-orbit term, it is obvious that a slight increase or decrease in γ leads to a slight increase or decrease in the overall spin-orbit FSI effect, independent of the specific kinematics. We therefore focus on b_s and ρ_s . As the fifth response is most sensitive to the spin-orbit FSI,

we choose it as a testing ground. Before checking the sensitivity to the NN parameters, it is useful to consider the spin-orbit FSI effect on the proton and the neutron separately. In Fig. 10, the solid line shows the fifth response calculated with the full FSI, i.e. with the spin-orbit FSI acting both on proton and neutron. The dashed line shows the results with the spin-orbit FSI acting on the proton only. One can see that the qualitative agreement between the curves is good. Naturally, the influence of the spin-orbit FSI on the neutron is largest when the fifth response changes sign, but for small missing momenta $p_m < 0.5 \text{ fm}^{-1}$ and the high missing momentum tail, $p_m > 1.8 \text{ fm}^{-1}$, its role is minor. The situation changes when we switch off the spin-orbit FSI on the proton, and keep only the spin-orbit FSI on the neutron, as depicted by the dash-dotted line: the results are qualitatively similar to the results with central FSI only (dotted line) — indeed, they are even somewhat smaller.

Note that here the case is different from proton-nucleus scattering, where the spin-orbit FSI on the spectator nucleon does not contribute for spin-0 targets. Here, it does contribute, although its contribution is much smaller than that of the spin-orbit FSI on the proton. This asymmetry is introduced in the problem by the assumption of the impulse approximation, i.e. the assumption that the nucleon with which the virtual photon interacted is the one which is detected later. This means that the electromagnetic current operator acts only on the proton, and therefore the spin-effects on proton and neutron cannot be the same, as the electromagnetic current operator contains spin-flipping parts. For the conditions we assume here, namely a very energetic virtual photon and a very energetic proton ($T_p = 1 \text{ GeV}$) which is measured, the impulse approximation is a realistic assumption, because it is quite unlikely that after its interaction with the photon the nucleon will transfer the momentum and energy gained in the hard vertex completely to the other nucleon. For lower energies, where both the proton and neutron in the final state have similar momenta, the Born graph does contribute and the spin-orbit FSI on the neutron should gain importance, as the situation then is more symmetric for the two nucleons.

In view of the importance of the spin-orbit FSI on the proton and the relatively small role of the spin-orbit FSI on the neutron, we will only discuss the sensitivity to the different NN parameters for the spin-orbit FSI on the proton. As the effects there are large, this should allow for the easy identification of the effects of changes in b_s and ρ_s . We start with different values of ρ_s for the proton, keeping all of the other NN parameters the same. The results of a calculation with $\rho_s = -0.44$ (the value we used for all of the above calculations) are compared to the results of a calculation with $\rho_s = +0.44$ in Fig. 11. The results are very similar to each other, the only significant deviations occurring in the region where $R_{TL'}$ changes its sign. We conclude that even the very drastic change of 200% in the value of ρ_s does not alter the results qualitatively and even does not alter the results quantitatively, except for the region of $1.3 \text{ fm}^{-1} < p_m < 2 \text{ fm}^{-1}$, where the response has a zero and any slight change in the calculation must induce a visible difference. So, although the value of ρ_s is not known with much precision, this uncertainty does not influence the practical calculations in a significant way.

In Fig. 12 we investigate the influence of the slope parameter value on the fifth response. The solid line shows the result with $\Re(b_s) = 0.65 \text{ fm}$, while the dashed line represents the results for $\Re(b_s) = 0.71 \text{ fm}$, which makes the interaction even longer-ranged. As expected, and as observed for the central FSI and the slope parameter b_o in [18], the longer-ranged interaction decreases the result at higher missing momenta. Consequently, the shorter-

ranged values of b_s lead to a slightly increased result at higher missing momenta, namely the dash-dotted curve for $\Re(b_s) = 0.59$ fm and the dotted curve for $\Re(b_s) = 0.52$ fm. On an absolute scale, these changes are small and they are present only for $p_m > 1.5$ fm $^{-1}$.

From these observations on the sensitivity to the NN parameters, we can conclude that the overall effect of the boost from the c.m. frame of the NN system to the lab frame only has a small effect, quite similar to the observations made in [19] for proton-nucleus scattering and the transformation from the c.m. to the Breit system. Also, the change in the parameters due to the boost is smaller than the uncertainty in the value of the parameter. Although the differences introduced by changing one NN parameter at a time are small, we found that a simultaneous change in the values of all NN parameters can add up to a significant shift of the zero of the fifth response.

In this paper, we did not consider double-spin-flip terms in the FSI. They are smaller than the spin-orbit term, and in the proton-nucleus Glauber calculations they are usually neglected. We estimate that their influence on the observables calculated here will be very small, since the spin-orbit FSI already allow the “big” components of the current and the wave function to contribute. Specifically, in the fifth response the contribution of the interference between magnetization current and zeroth-order charge operator is the biggest contribution one can expect, and it is already present when the spin-orbit FSI is included. However, there may be other observables, e.g. double polarization observables, where the double-spin-flip FSI might contribute — in these cases, it will be necessary to re-examine many of the approximations made in the present study.

V. SUMMARY AND OUTLOOK

The final-state interactions have a rich structure: due to the short-ranged nature of the central part of the FSI, they tend to smear out the differences between the various theoretical models for the nuclear ground state. Our results indicate that one of the smaller responses or a polarization observable might be better suited for this purpose. A reliable theoretical calculation of these responses must include the spin-orbit FSI as well as the central FSI. We have included the spin-orbit FSI, for the fifth response function showing that the spin-dependent FSI is indeed crucial. The calculations presented here go beyond the approach usually taken in calculations for $(e, e'p)$ reactions in the framework of Glauber theory, where only the central FSI is included. In addition, we have pointed out that due to the longer-ranged nature of the spin-orbit final-state interaction, the FSI can also have a significant impact on the D-wave contribution. The experimental measurement of the small responses and the polarization observables is a challenge that holds potential to shed light on interesting issues involving all of the ingredients in electronuclear physics, namely, initial- and final-state nuclear structure and electromagnetic operators. Of specific relevance for the present work, we note that the fifth response function will be measured for a variety of nuclei at Jefferson Lab in the near future [21].

ACKNOWLEDGMENTS

S. J. thanks N. N. Nikolaev and R. Schiavilla for useful comments on the manuscript. S.J. is grateful to the Alexander von Humboldt Foundation for financial support during part of this work. This work was in part supported by funds provided by the U.S. Department of Energy (D.O.E.) under cooperative research agreement #DF-FC02-94ER40818 and #DE-AC05-84ER40150.

APPENDIX A: RESPONSE FUNCTIONS AND CURRENT OPERATOR

For the convenience of the reader, we provide the definition of the response functions and identify the different parts of the electromagnetic current. For more information on exclusive electron scattering in general, the reader is referred to [22]; for the electromagnetic current operator and the relativistic effects incorporated in it, see [4].

The differential cross section is equal to

$$\left(\frac{d\sigma^5}{d\epsilon' d\Omega_e d\Omega_N} \right)_{fi}^h = \frac{m_N m_f p_N}{8\pi^3 m_i} \sigma_{Mott} f_{rec}^{-1} \left[(v_L R_{fi}^L + v_T R_{fi}^T + v_{TT} R_{fi}^{TT} + v_{TL} R_{fi}^{TL}) + h (v_{T'} R_{fi}^{T'} + v_{TL'} R_{fi}^{TL'}) \right], \quad (A1)$$

where m_i , m_N and m_f are the masses of the target nucleus, the ejectile nucleon and the residual system, p_N and Ω_N are the momentum and solid angle of the ejectile, ϵ' is the energy of the detected electron and Ω_e is its solid angle. The helicity of the electron is denoted by h . The coefficients v_K are the leptonic coefficients, and the R_K are the response functions which are defined by

$$\begin{aligned} R_{fi}^L &\equiv |\rho(\vec{q})_{fi}|^2 \\ R_{fi}^T &\equiv |J_+(\vec{q})_{fi}|^2 + |J_-(\vec{q})_{fi}|^2 \\ R_{fi}^{TT} &\equiv 2 \Re [J_+^*(\vec{q})_{fi} J_-(\vec{q})_{fi}] \\ R_{fi}^{TL} &\equiv -2 \Re [\rho^*(\vec{q})_{fi} (J_+(\vec{q})_{fi} - J_-(\vec{q})_{fi})] \\ R_{fi}^{T'} &\equiv |J_+(\vec{q})_{fi}|^2 - |J_-(\vec{q})_{fi}|^2 \\ R_{fi}^{TL'} &\equiv -2 \Re [\rho^*(\vec{q})_{fi} (J_+(\vec{q})_{fi} + J_-(\vec{q})_{fi})], \end{aligned} \quad (A2)$$

where the J_{\pm} are the spherical components of the current. For our calculations, we have chosen the following kinematic conditions: the z-axis is parallel to \vec{q} , the missing momentum is defined as $\vec{p}_m \equiv \vec{q} - \vec{p}_N$, so that in PWIA, the missing momentum is equal to the negative initial momentum of the struck nucleon in the nucleus, $\vec{p}_m = -\vec{p}$. We denote the angle between \vec{p}_m and \vec{q} by θ , and the term “parallel kinematics” indicates $\theta = 0^\circ$, “perpendicular kinematics” indicates $\theta = 90^\circ$, and “antiparallel kinematics” indicates $\theta = 180^\circ$. Note that both this definition of the missing momentum and the definition with the other sign are used in the literature. In this paper, we assume that the experimental conditions are such that the kinetic energy of the outgoing nucleon and the angles of the missing momentum,

θ and the azimuthal angle ϕ , are fixed. The kinetic energy of the outgoing proton is fixed to 1 GeV. For changing missing momentum, the transferred energy and momentum change accordingly.

The electromagnetic current operator

$$J^\mu(P\Lambda; P'\Lambda') = \bar{u}(P'\Lambda') \left[F_1 \gamma^\mu + \frac{i}{2m_N} F_2 \sigma^{\mu\nu} Q_\nu \right] u(P\Lambda) \quad (\text{A3})$$

can be rewritten in a form that is more suitable for application to nuclear problems:

$$J^\mu(P\Lambda; P'\Lambda') \equiv \chi_{\Lambda'}^\dagger \bar{J}^\mu(P; P') \chi_\Lambda \quad (\text{A4})$$

with

$$\begin{aligned} \bar{J}^o &= \rho = f_o (\xi_o + i \xi'_o (\vec{q} \times \vec{p}) \cdot \vec{\sigma}) \\ \bar{J}^3 &= \frac{\omega}{q} \bar{J}^o \\ \bar{J}^\perp &= f_o \left(\xi_1 \left[\vec{p} - \left(\frac{\vec{q} \cdot \vec{p}}{q^2} \right) \vec{q} \right] - i \{ \xi'_1 (\vec{q} \times \vec{\sigma}) \right. \\ &\quad \left. + \xi'_2 (\vec{q} \cdot \vec{\sigma}) (\vec{q} \times \vec{p}) + \xi'_3 [(\vec{q} \times \vec{p}) \cdot \vec{\sigma}] \left[\vec{p} - \left(\frac{\vec{q} \cdot \vec{p}}{q^2} \right) \vec{q} \right] \} \right). \end{aligned} \quad (\text{A5})$$

Here, f_o, ξ_i, ξ'_i are all functions of ω, q, p^2 ; their explicit forms are given in [4]. For the reasons explained in [4], we refer to the operator associated with ξ_o as zeroth-order charge operator, we call the term containing the ξ'_o first-order spin-orbit operator, the term containing ξ_1 first-order convection current, the term containing ξ'_1 zeroth-order magnetization current, the term containing ξ'_2 first-order convective spin-orbit term, and the term containing ξ'_3 second-order convective spin-orbit term. In this paper, we have used the current expanded up to first order in the initial nucleon's momentum and retained terms of all order in the transferred energy ω and the transferred momentum q .

Note that we retain more terms in the current than with the commonly used strict nonrelativistic reduction, which assumes that the transferred momentum q is smaller than the nucleon mass, and that both the initial nucleon momentum and the transferred energy are smaller than q and therefore much smaller than the nucleon mass. Under these assumptions, the current operator simplifies to the form

$$\begin{aligned} \bar{J}_{\text{nonrel}}^o &= G_E \\ \bar{J}_{\text{nonrel}}^\perp &= -\frac{i}{2m_N} G_M (\vec{q} \times \vec{\sigma}) + \frac{1}{m_N} G_E \left(\vec{p} - \frac{\vec{q} \cdot \vec{p}}{q^2} \vec{q} \right), \end{aligned}$$

which contains only the zeroth-order charge operator, the zeroth-order magnetization current and the first-order convection current.

REFERENCES

- [1] E. Hummel and J. A. Tjon, *Phys. Rev. C* **49**, 21 (1994).
- [2] J. W. Van Orden, N. Devine and F. Gross, *Phys. Rev. Lett.* **75**, 4369 (1995).
- [3] F. Gross, proceedings of the Workshop on Electronuclear Physics with Internal Targets and the BLAST Detector, (MIT, May, 1998).
- [4] S. Jeschonnek and T.W. Donnelly, *Phys. Rev. C* **57**, 2438 (1998).
- [5] R. Machleidt, K. Holinde and C. Elster, *Phys. Rep.* **149**, 1 (1987).
- [6] M. Lacombe, B. Loiseau, R. Mau, J. Côté, P. Pirès and R. Tourreil, *Phys. Lett.* **B101**, 139 (1981).
- [7] V.G.J. Stoks, R.A.M. Klomp, C.P.F. Terheggen and J.J. de Swart, *Phys. Rev. C* **49**, 2950 (1994).
- [8] R. J. Glauber, in *Lectures in Theoretical Physics*, Vol. 1, edited by W. Brittin and L. G. Dunham (Interscience Publ., New York, 1959).
- [9] C. Lechanoine-Leluc and F. Lehar, *Rev. Mod. Phys.* **65**, 47 (1993).
- [10] R. J. Glauber and G. Matthiae, *Nucl. Phys.* **B21**, 135 (1970).
- [11] S. J. Wallace, *Adv. Nucl. Phys.* **12**, 135 (1981).
- [12] G. D. Alkhazov, S. L. Belostotsky and A. A. Vorobyov, *Phys. Rep.* **42**, 89 (1978).
- [13] A. Bianconi, S. Jeschonnek, N. N. Nikolaev and B. G. Zakharov, *Phys. Lett.* **B343**, 13 (1995).
- [14] A. Bianconi, S. Jeschonnek, N. N. Nikolaev and B. G. Zakharov, *Phys. Rev. C* **53**, 576 (1996).
- [15] L. L. Frankfurt, M. M. Sargsian and M. I. Strikman, *Phys. Rev. C* **56**, 1124 (1997); L. L. Frankfurt, W. R. Greenberg, G.A. Miller, M. M. Sargsian and M. I. Strikman, *Z. Phys. A* **352**, 97 (1995).
- [16] A. Kohama, K. Yazaki and R. Seki, *Nucl. Phys.* **A551**, 687 (1993).
- [17] H. Ito, S. E. Koonin and R. Seki, *Phys. Rev. C* **56**, 3231 (1997).
- [18] S. Jeschonnek, Ph.D. thesis, Bonn 1996,
Berichte des Forschungszentrums Jülich, Vol. 3175, ISSN 0944-2952. Also available at:
<http://www-ctp.mit.edu/~jeschonn/home.html>
- [19] J. A. McNeil, L. Ray and S. J. Wallace, *Phys. Rev. C* **27**, 2123 (1983).
- [20] V. Franco and R. J. Glauber, *Phys. Rev.* **142**, 1195 (1966).
- [21] M. Holtrop and F. W. Hersman (co-spokespersons), Jefferson Lab Experiment PR98-104, *Measurement of the polarized electron beam asymmetry in exclusive reactions on nuclei with CLAS*.
- [22] A. S. Raskin and T. W. Donnelly, *Ann. of Phys.* **191**, 78 (1989).

TABLES

TABLE I. NN amplitude parameters for the central and spin-orbit terms from the Glauber proton-nucleus scattering analysis. Parameters are given in the NN c.m. frame.

σ_{tot}^{NN} / mb	b_o / fm	ρ	γ / fm	b_s / fm	ρ_s
41.1	0.48	-0.48	0.16	0.65	-0.24

TABLE II. NN amplitude parameters for the central and spin-orbit terms from the phase shift analysis analysis. Parameters are given in the NN c.m. frame.

σ_{tot}^{NN} / mb	b_o / fm	ρ	γ / fm	b_s / fm	ρ_s
36.9	0.57 - i 0.07	-0.47	0.20	0.53 + i 0.05	0.52

TABLE III. NN amplitude parameters for the spin-orbit terms from the Glauber proton-nucleus scattering analysis. Parameters are given in the NN lab frame.

nucleon	γ / fm	b_s / fm	ρ_s
proton	0.15	0.65 - i 0.03	-0.44
neutron	0.17	0.64 - i 0.03	-0.02

TABLE IV. NN amplitude parameters for the spin-orbit terms from the NN phase shift analysis. Parameters are given in the NN lab frame.

nucleon	γ / fm	b_s / fm	ρ_s
proton	0.18	0.53 + i 0.07	0.41
neutron	0.21	0.52 + i 0.03	0.64

FIGURES

FIG. 1. Schematic representation of the $(e, e'N)$ reaction. The electron exchanges a photon with the nucleus, and the photon knocks out a nucleon which undergoes final-state interactions (FSI) while leaving the nucleus. The scattered electron and the nucleon are detected in coincidence. The other hadrons in the final state remain unobserved.

FIG. 2. Panel (a) shows the nucleon momentum distribution $n(p)$ for the deuteron calculated with the Bonn wave function (solid line) and the Paris wave function (dashed line). Panel (b) shows the decomposition of the full nucleon momentum distribution calculated with the Bonn wave function (solid line) into the S-wave part (dashed line) and the D-wave part (dash-dotted line).

FIG. 3. On the left, the five-fold differential cross section for the reaction $D(e, e'p)n$ is shown in parallel kinematics (the angle of the missing momentum $\vartheta = 0^\circ$), on the right, it is shown for perpendicular kinematics ($\vartheta = 90^\circ$). The solid line shows the calculation including central FSI, while the dashed line shows the PWIA result. The beam energy is 6 GeV.

FIG. 4. On the left, the five-fold differential cross section for the reaction $D(e, e'p)n$ is shown in PWIA; on the right it is shown including central FSI. The top panels show the cross section in parallel kinematics, whereas the bottom panels show it in perpendicular kinematics. The solid line shows the calculation performed with the Bonn wave function, while the dashed line is the Paris wave function result. The beam energy is 6 GeV.

FIG. 5. The top panels, (a) and (b), show the absolute value of the transverse-longitudinal response function R_{TL} , while the bottom panels, (c) and (d), show the absolute value of the transverse-transverse response function R_{TT} . In all panels, the solid line shows the calculation including central FSI. The dashed line in (a) and (c) shows the PWIA result, whereas the dashed line in (b) and (d) shows the S-wave contribution and the dash-dotted line in (b) and (d) shows the D-wave contribution. The total response R_{TT} is negative over the entire p_m range, as is its S-wave part. The D-wave part is positive for missing momenta less than 0.5 fm^{-1} and then turns negative, too. The total response R_{TL} is positive over the entire p_m range, as is its D-wave part. The S-wave part is negative from 1.4 fm^{-1} to 2.1 fm^{-1} .

FIG. 6. The real part (left panel) and the absolute value of the imaginary part (right panel) of the central profile function (solid line) in coordinate space for pn scattering at $T_{lab} = 1 \text{ GeV}$ and the spin-orbit profile function (dashed line). The profile functions are plotted versus the transverse separation b of the two nucleons. The parameters for the central part are $\sigma_{tot}^{pn} = 41.1 \text{ mb}$, $b_o = 0.48 \text{ fm}$, and $\rho = -0.48$. For the spin-orbit part, we use $\gamma = 0.16 \text{ fm}$, $b_s = 0.65 \text{ fm}$ and $\rho_s = -0.24$. The imaginary part of the spin-orbit profile function is negative and the imaginary part of the central profile function is positive.

FIG. 7. The top panels, (a) and (b), show the absolute value of the transverse-longitudinal response function R_{TL} , while the bottom panels, (c) and (d), show the absolute value of the transverse-transverse response function R_{TT} . In all panels, the solid line shows the calculation including central and spin-orbit FSI. The dashed line in (a) and (c) shows the central FSI result, and the dash-dotted line in (a) and (c) shows the PWIA result. In panels (b) and (d), the dashed line shows the S-wave contribution and the dash-dotted line shows the D-wave contribution. The full response R_{TT} is negative, except for $1.2 \text{ fm}^{-1} < p_m < 1.5 \text{ fm}^{-1}$. Its S-wave part is negative over the entire p_m range, and its D-wave part is positive over the entire p_m range. The full response R_{TL} is positive over the entire p_m range, as is its D-wave part. The S-wave part is negative from 1.4 fm^{-1} to 2.1 fm^{-1} .

FIG. 8. On the left, the interference responses R_{TL} and R_{TT} are shown in PWIA; on the right they are shown including central and spin-orbit FSI, in both cases for perpendicular kinematics. The top panels show the transverse-longitudinal response function, and the bottom panels show the transverse-transverse response function. The solid line shows the calculation performed with the Bonn wave function, whereas the dashed line is the Paris wave function result.

FIG. 9. The fifth response function, $R_{TL'}$, is shown in panel (a) calculated with the full FSI (solid line) and with central FSI only (dashed line) in perpendicular kinematics at an azimuthal angle $\varphi = 90^\circ$. The full response is negative for $p_m < 1.4 \text{ fm}^{-1}$; with central FSI only, it is positive up to $p_m = 2.6 \text{ fm}^{-1}$. Panel (c) shows the response calculated including full FSI with the Bonn wave function (solid line) and the Paris wave function (dashed line). In panels (b) and (d), besides the full response (solid line), we show the S-wave part (dashed line) and the D-wave part (dash-dotted) for the calculation with central FSI (d) and full FSI (b).

FIG. 10. The fifth response function, $R_{TL'}$, is shown in perpendicular kinematics at an azimuthal angle $\varphi = 90^\circ$. The various curves represent a calculation with the full FSI (solid line), a calculation with central FSI and spin-orbit FSI only on the proton (dashed line), a calculation with central FSI and spin-orbit FSI only on the neutron (dash-dotted line), and a calculation with central FSI only (dotted line).

FIG. 11. The fifth response function, $R_{TL'}$, is shown in perpendicular kinematics at an azimuthal angle $\varphi = 90^\circ$. The solid line shows the results of the calculation with $\rho_s = -0.44$ for the proton, while the dashed line shows the result for the changed sign of ρ_s , i.e. for $\rho_s = +0.44$.

FIG. 12. The fifth response function, $R_{TL'}$, is shown in perpendicular kinematics at an azimuthal angle $\varphi = 90^\circ$. The solid line shows the results of the calculation with $\Re(b_s) = 0.65 \text{ fm}$ for the proton, the dashed line shows the result for $\Re(b_s) = 0.71 \text{ fm}$, the dash-dotted line corresponds to $\Re(b_s) = 0.59$, and the dotted line represents $\Re(b_s) = 0.52$.

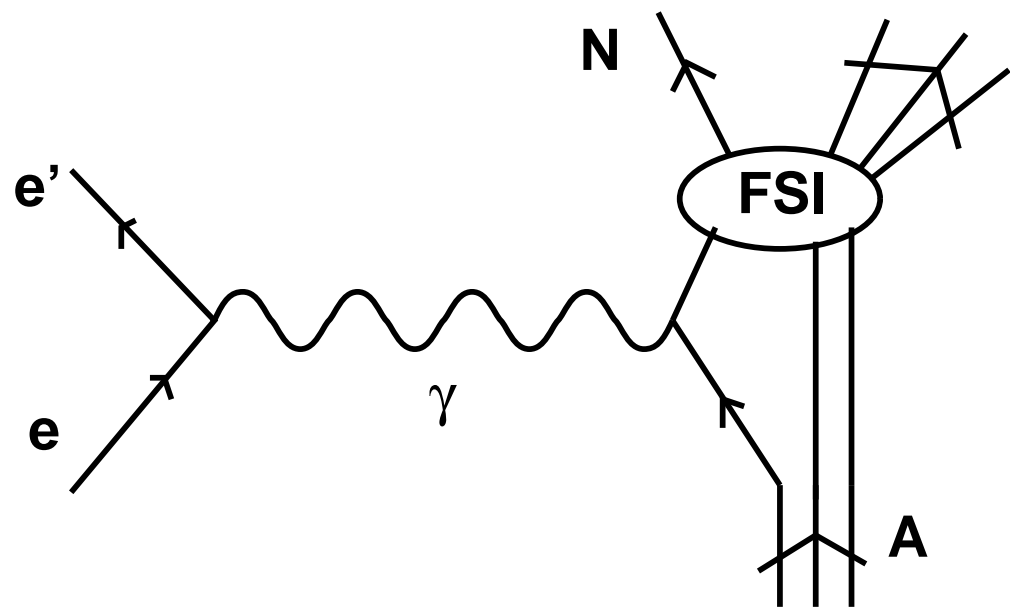


Figure 1

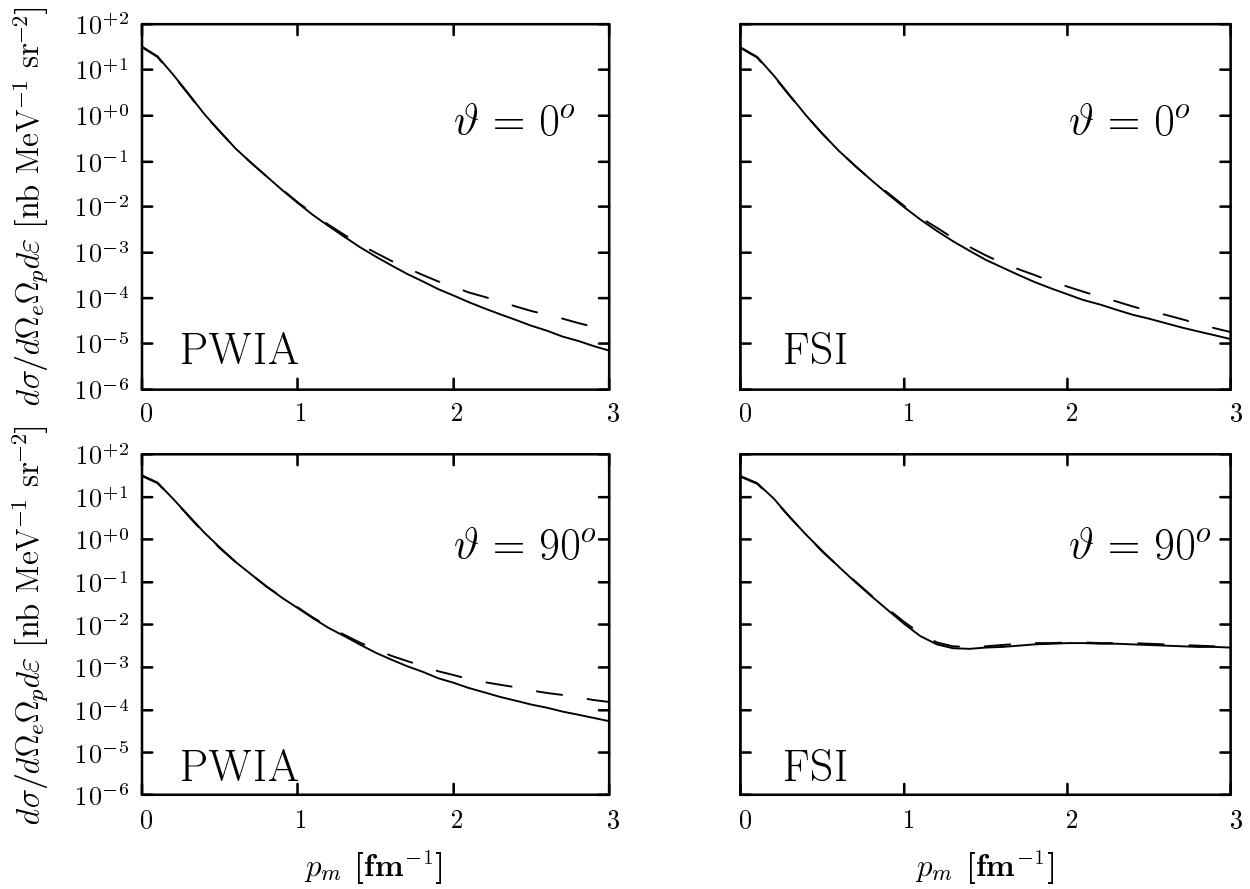


Figure 4

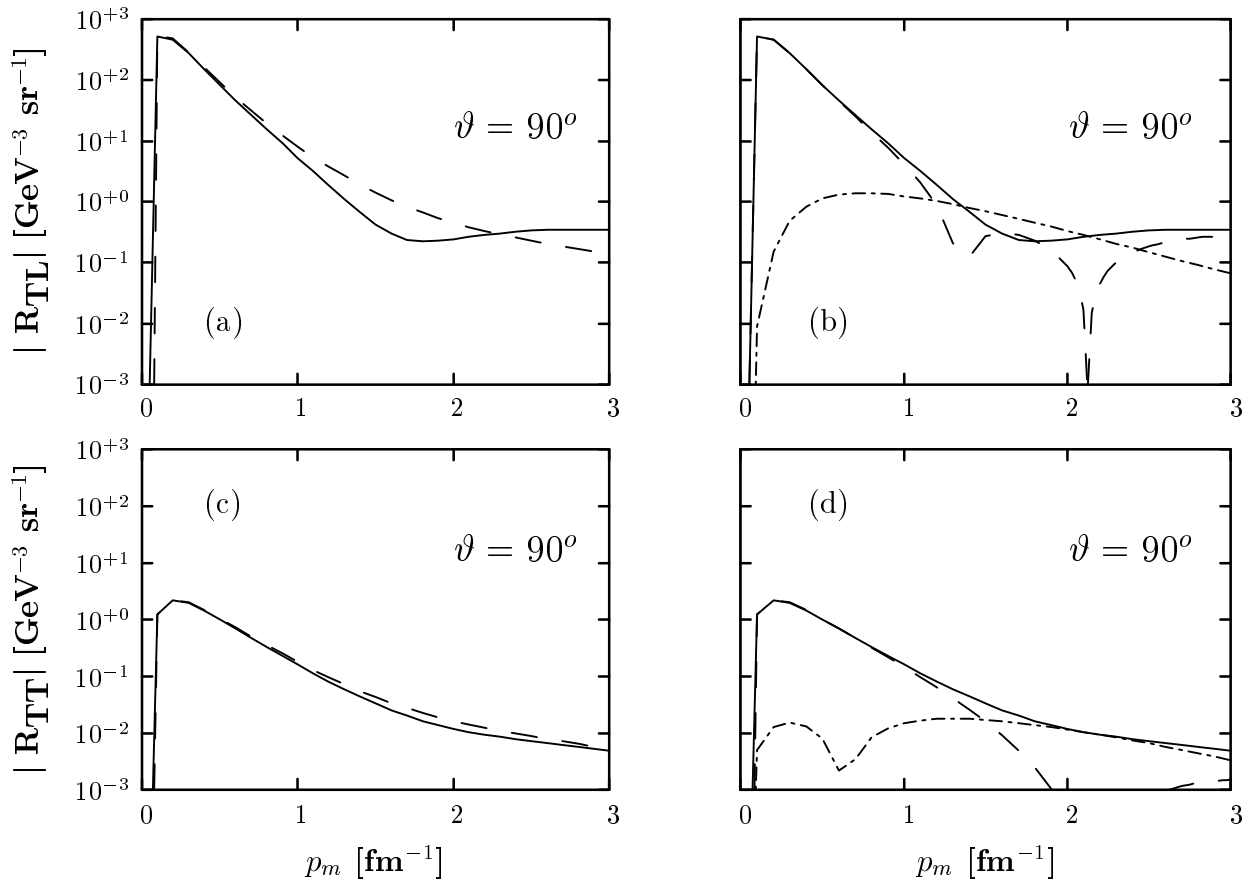


Figure 5

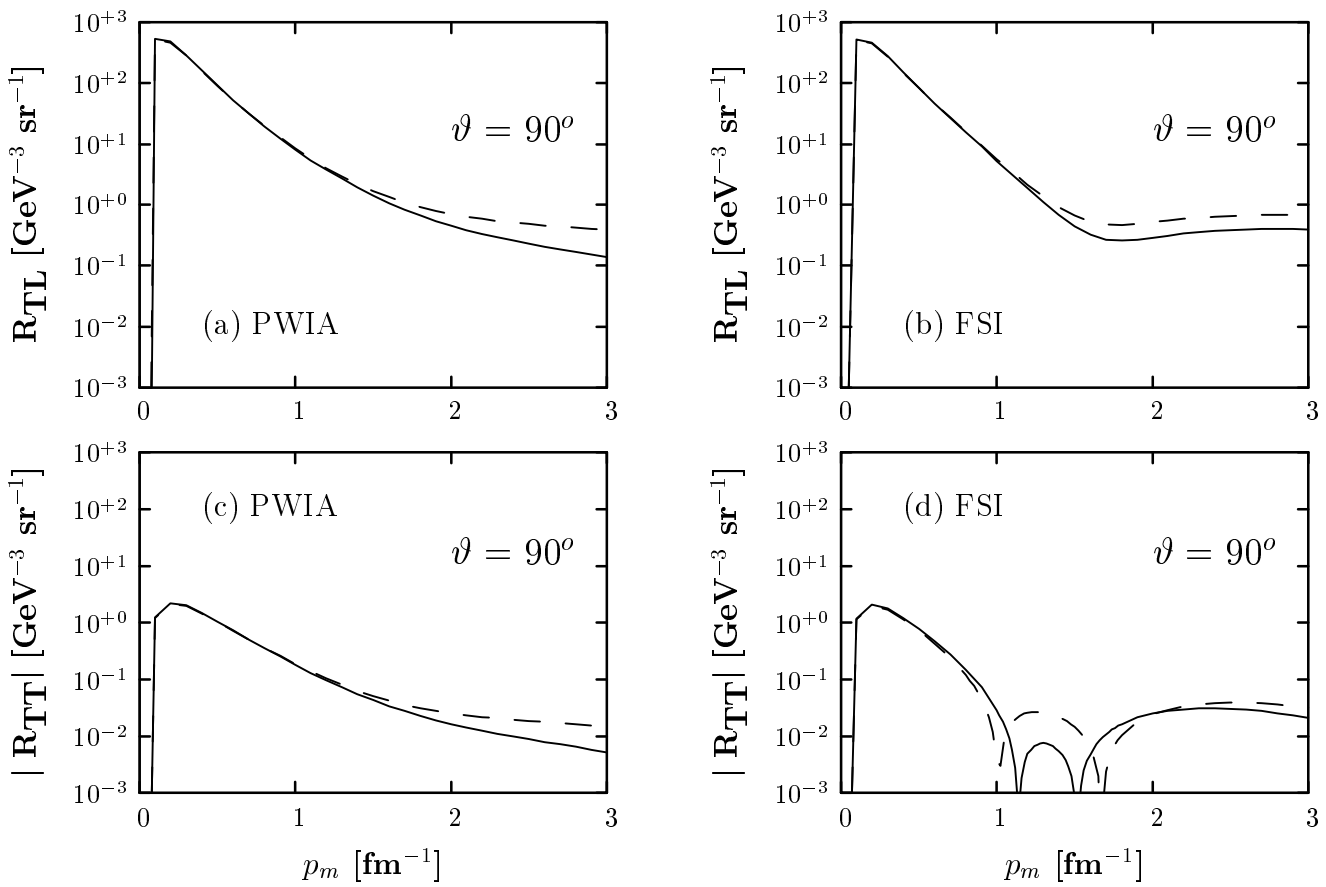


Figure 8

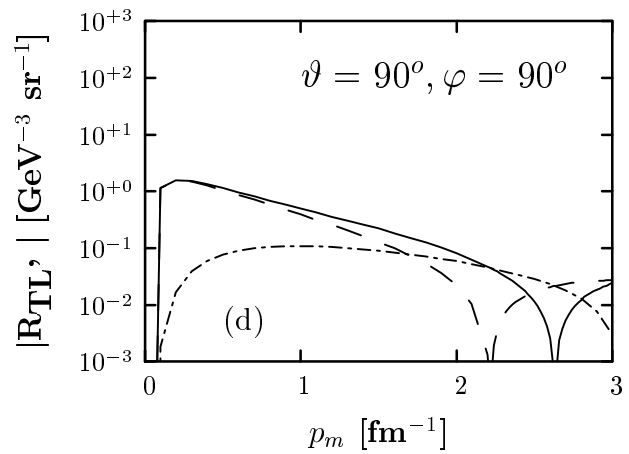
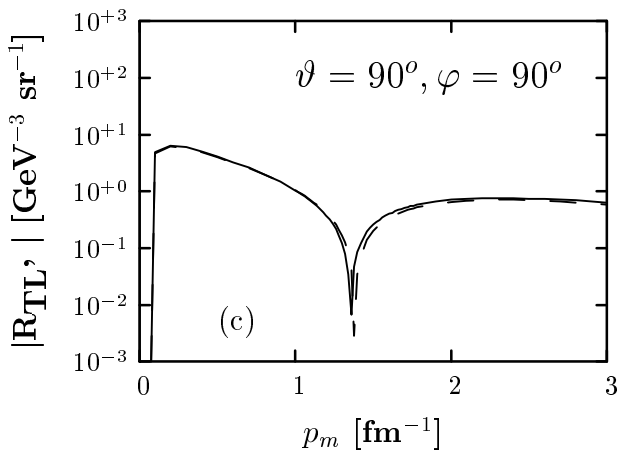
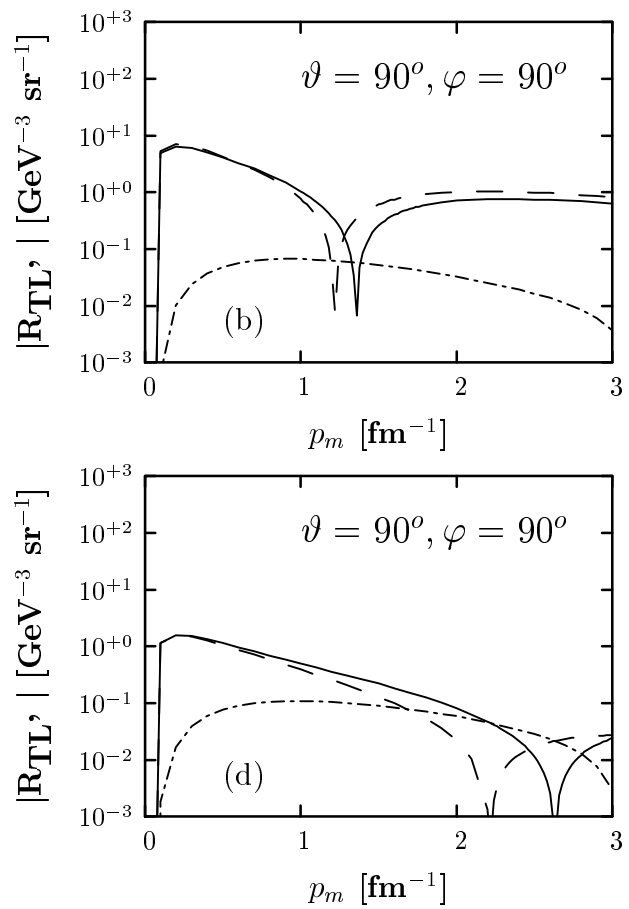
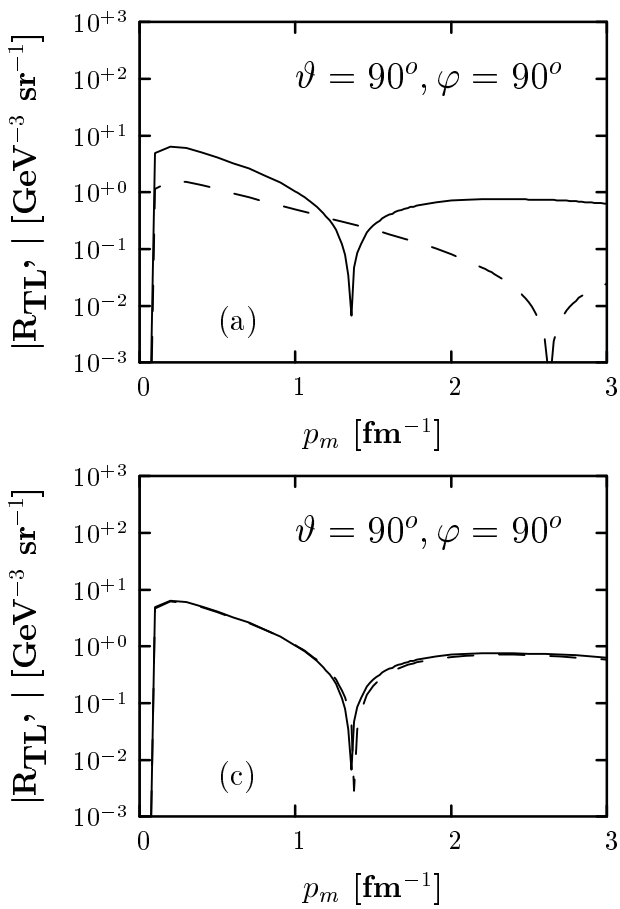


Figure 9

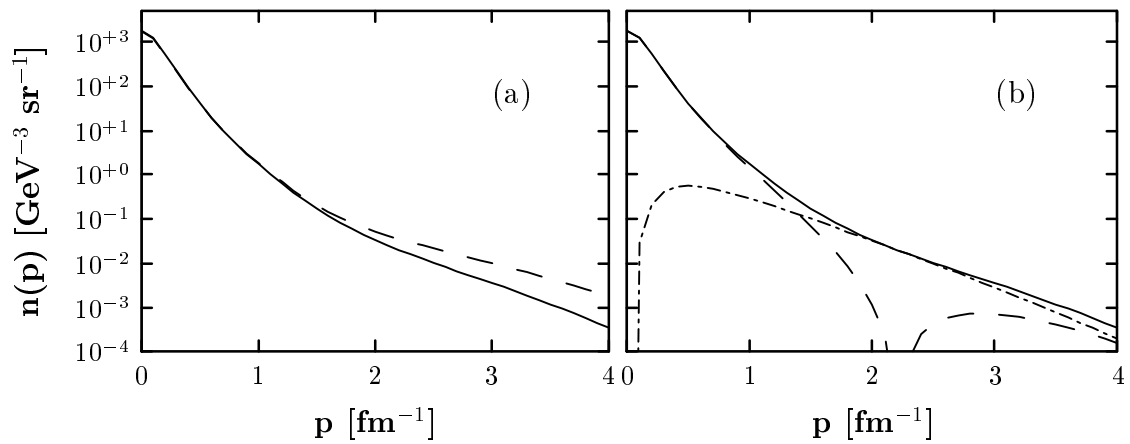


Figure 2

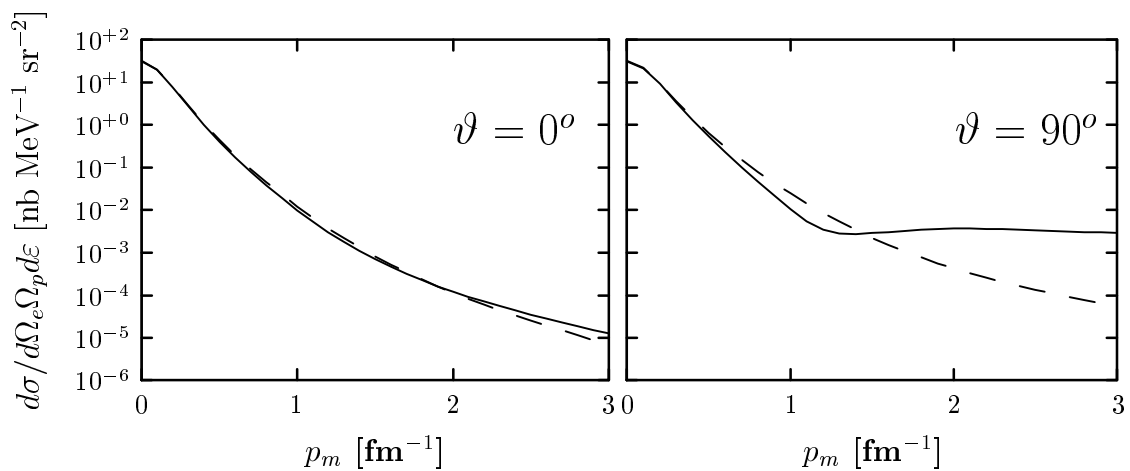


Figure 3

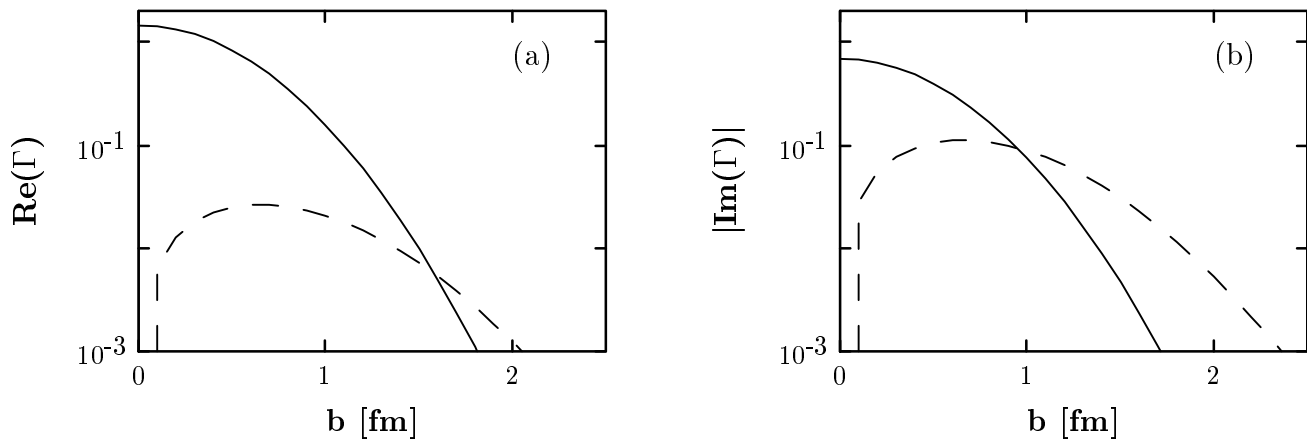


Figure 6

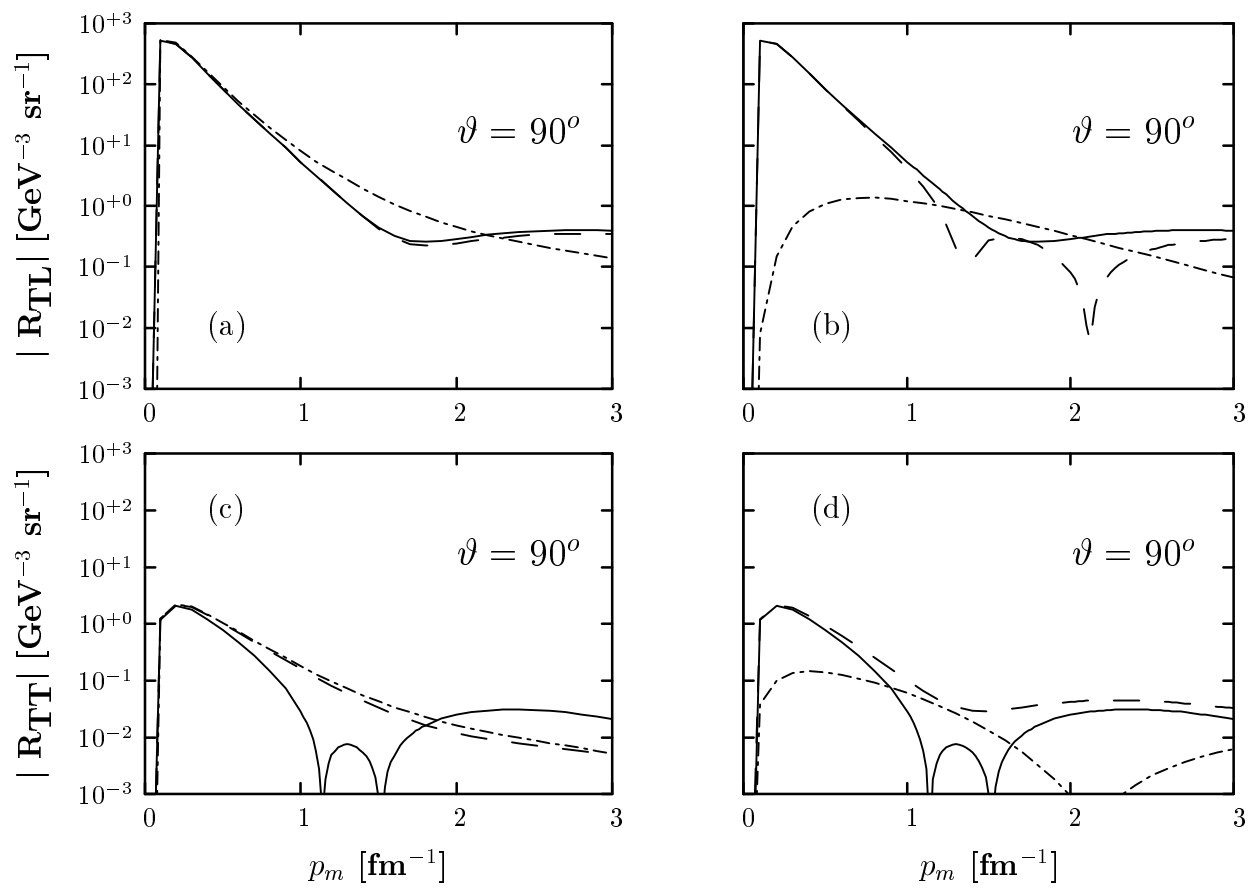


Figure 7

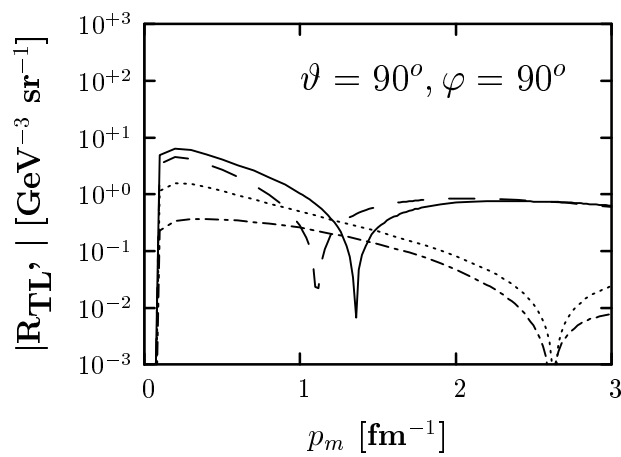


Figure 10

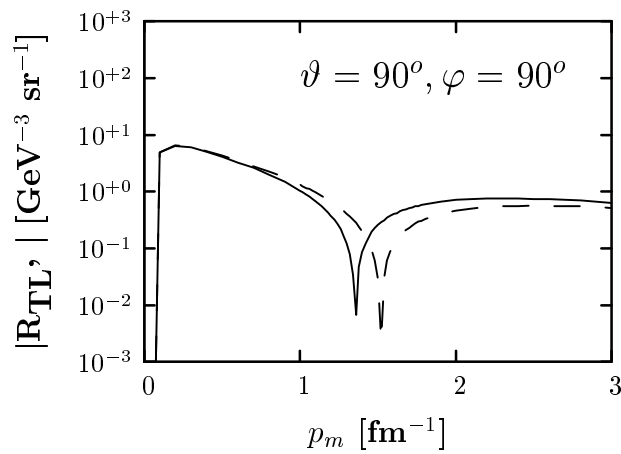


Figure 11

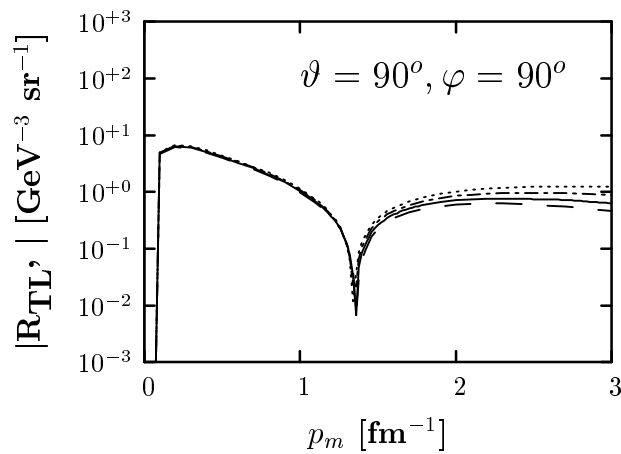


Figure 12